

# Ions modulate stress-induced nano-texture in supported fluid lipid bilayers

Luca Piantanida<sup>1</sup>, Hannah L. Bolt<sup>2</sup>, Neshat Rozatian<sup>2</sup>, Steven L. Cobb<sup>2</sup>, Kislun Voïtchovsky<sup>1\*</sup>

<sup>1</sup>Department of Physics and <sup>2</sup>Department of Chemistry, Durham University, South Road, Durham, DH1 3LE, UK.

## ABSTRACT

Most plasma membranes comprise a large number of different molecules including lipids and proteins. In the standard ‘fluid mosaic’ model, the membrane function is ensured by proteins while lipids are largely passive and serve solely to the membrane cohesion. Here we show, using supported 1,2-dioleoyl-sn-glycero-3-phosphocholine (DOPC) lipid bilayers in different saline solutions, that ions can locally induce ordering of the lipid molecules within the otherwise fluid bilayer when the latter is supported. This nano-ordering exhibits a characteristic lengthscale of ~20 nm, and manifests itself clearly when mechanical stress is applied to the membrane. Atomic force microscopy (AFM) measurements in aqueous solutions containing NaCl, KCl, CaCl<sub>2</sub> and Tris buffer show that the magnitude of the effect is strongly ion-specific, with Ca<sup>2+</sup> and Tris respectively promoting and reducing stress-induced nano-texturing of the membrane. The AFM results are complemented by fluorescence recovery after photobleaching (FRAP) experiments, which reveal an inverse correlation between the tendency for molecular nano-ordering and the diffusion coefficient within the bilayer. Control AFM experiments on other lipids and at different temperatures support the hypothesis that the nano-texturing is induced by reversible, localized gel-like solidification of the membrane. These results suggest that supported fluid phospholipid bilayers are not homogenous at the nanoscale, but specific ions are able to locally alter molecular organisation and mobility, and spatially modulate the membrane’s properties on a lengthscale of ~20 nm. To further illustrate this point, we followed with AFM the adsorption of the membrane-penetrating antimicrobial peptide Temporin L in different solutions. The results confirm that the peptides do not absorb randomly, but follow the ion-induced spatial modulation of the membrane. Our results suggest that ionic effects have a significant impact for passively modulating the local properties of biological membranes, where in contact with a support such as the cytoskeleton.

## INTRODUCTION

The plasma membrane separates the inside of the cell from the surrounding environment. It is a highly organized and heterogeneous structure composed of phospholipids, proteins and organic molecules (1), and plays a fundamental and active role in the cell function. The lipids, which are the main constituent of the membrane, form a fluid double layer that embeds and anchors active biomolecules. The interplay between lipids and host molecules in the membrane is however still poorly understood. The first widely accepted membrane model (2), the so-called “fluid mosaic” model, assumes that phospholipids are merely structural molecules in which membrane proteins can move freely. This passive description of the membrane lipids is increasingly challenged by recent findings (3-6). Studies have shown that the membrane is a highly dynamical structure that actively supports the cell function. Phospholipids play an important role in this new understanding, for example in conferring membrane curvature (7) and actively organizing proteins complexes (6, 8). Despite these advances, our molecular-level understanding of plasma membranes is still limited, partly due to a lack of experimental results. Important questions related to the anomalous diffusion of lipids under certain circumstances (9, 10) or the role of membrane rafts (11) remain a matter of debate. Molecular-level studies of natural biomembranes are usually challenging due to the large number of different molecules in the membrane as well as their specific organisation. In order to overcome these difficulties, many studies make use of synthetic lipid bilayers as model biological membranes. The advantage of synthetic bilayers is the possibility of controlling the membrane composition precisely, therefore helping the interpretation of experiments while retaining some of the most important features of natural biomembranes (12-15). Additionally, when addressing single-molecule details, it is often helpful to support the membrane on a substrate. In cells, free standing plasma

1 membranes constantly reshape (16) and undulate (17) in order to help cellular function, rendering local tracking  
2 of molecules challenging. Solid-supported membranes are typically immersed in aqueous solution, and only a  
3 few nanometres of the solution separate the membrane from the solid support (18). This approach effectively  
4 confines the membrane in two dimensions, hence facilitating high-resolution investigations with techniques such  
5 as atomic force microscopy (19), fluorescence microscopy (20), fluorescence recovery after photobleaching  
6 (21), quartz crystal microbalance (22) and neutron reflectometry (6). Synthetic supported lipid bilayers (23)  
7 (SLBs) are routinely used in experimental studies, including for investigating the influence of proteins (24, 25),  
8 antibodies (26), functionalized nanoparticles (27), polymers (28), amino acids (29) and antimicrobial peptides  
9 (30) on the morphology and biophysical properties of the membrane.

10 The presence of a supporting solid does, however, affect the behaviour of SLBs. Simple biophysical properties  
11 such as the lipids transition temperature (31) and molecular diffusion coefficients have been shown to differ in  
12 SLBs when compared with identical membranes freestanding in solution (23). This can be partly explained by  
13 interactions between the lipids of SLBs and the substrate. These interactions can be direct such as van der Waals  
14 and electrostatic forces (12, 32), or indirect, through a global hydrogen bond network that stabilises the  
15 membrane when immersed in a solution. The hydrophilicity of the substrate can affect the thickness and the  
16 dynamics of the water trapped between the substrate and the bilayer (33). Not surprisingly, the formation and  
17 properties of SLBs can be tuned by changes in the lipid-substrate interactions, for example through the  
18 solution's pH (34), ionic strength (35), electrolyte content (36-38), by temperature (39), as well as the  
19 substrate's topography and chemistry (40). The fact that SLBs' properties differ from those of freestanding  
20 bilayers is often seen as a limitation of SLB-based experiments, with natural biomembranes expected to behave  
21 more like freestanding bilayers. However, natural cell membranes are never completely freestanding, but locally  
22 supported and constrained by the cytoskeleton and cytoplasm on one side, and the extracellular matrix on the  
23 other side. Local interactions between these supports and the molecules composing the membranes are believed  
24 to play an active role in the membrane function and to be key to the cell survival (41). The interaction of SLBs  
25 with the substrate therefore represents an opportunity to examine the influence of cell support on the local  
26 properties of the membrane. Given the extended and homogenous SLB-substrate interaction in most  
27 experiments, it is necessary to investigate the membrane locally, and at the nanoscale if results are to be relevant  
28 for our understanding of natural systems.

29 Atomic force microscopy (42) (AFM) is a tool of choice to conduct this type of experimental study; it operates  
30 locally at the nanoscale (43), can function in liquid environment (44), and can quantify not only topography (45)  
31 but also the nano-mechanical and viscoelastic properties (46) of soft biological samples. Studies of SLBs with  
32 AFM in liquid environment (19, 47) have allowed identification of nanoscale features such as different lipid  
33 microdomains (48), and sub-molecular details of membrane protein structure (49) and function (50). When  
34 operated dynamically (vibrating tip) and with small tip oscillation amplitudes, it is also possible to derive  
35 molecular-level information about the membrane hydration landscape (51) including in the presence of adsorbed  
36 ions (52, 53) that can often be directly imaged (54, 55). Recent AFM studies have shown that ions can form  
37 correlated clusters at the surface of mica in solution (56). Ions have long been known to interact with  
38 biomembranes (37, 57) and sometimes specifically with lipids (58). Metal cations can bind to different locations  
39 of the lipids headgroups of common plasma membrane's lipids such as phosphatidylcholine or  
40 phosphatidylserine (38, 59, 60). This often results in significant changes of the membrane's characteristics (61,  
41 62). The effect of ions on the substrate-bilayer interaction is however still poorly understood at the mesoscale –  
42 the 1-100 nm range– where correlation and clustering effects are expected to dominate (63). In that range, a  
43 small number of molecules acting in a coherent manner can induce local but significant changes in the  
44 membrane's properties. Furthermore, the role of macro-ions such as commonly used buffer molecules is  
45 generally ignored. Buffers and metal ions trapped between the substrate and the bilayer can significantly alter  
46 the hydration landscape of the proximal leaflet, potentially affecting the local nano-mechanics and dynamics of  
47 the supported lipid bilayer surface.

48 In this study we use AFM to investigate the effect of different metal and buffer ions on the interaction between  
49 fluid phospholipid SLBs with the underlying substrate in solution. We focus on the nanoscale organisation of  
50 the lipids when under local confinement. We show that the average pressure applied by the AFM tip while  
51 imaging the SLB could trigger the formation of long-lived but reversible mesoscale structures, likely due to a  
52 localised gelation-like ordering of lipid molecules in the membrane. This phenomenon depends strongly on the  
53 ionic species present in the solution used for creating the SLB. We correlate the AFM results with the average  
54 lateral diffusion coefficient of the lipids in the membrane, obtained from fluorescence recovery after  
55 photobleaching (FRAP) measurements. The results are discussed from the perspective of nanoscale lipid  
56 mobility and molecular interactions. We also discuss the importance of ion-induced mesoscale effects for

1 modulating the adsorption of biomolecules, illustrated here with the cell-penetrating antimicrobial peptide  
2 Temporin L.

## 6 MATERIALS AND METHODS

### 7 Materials

8 All chemicals were obtained from commercial sources and used without further purification. The lipids, 1,2-  
9 dioleoyl-sn-glycero-3-phosphocholine (DOPC), 1-palmitoyl-2-oleoyl-sn-glycero-3-phosphocholine (POPC),  
10 and 1,2-dioleoyl-sn-glycero-3-phospho-L-serine (DOPS) were purchased dissolved in chloroform from Avanti  
11 Polar Lipids Inc. (Alabaster, Alabama, USA). 1,2-dipalmitoyl-sn-glycero-3-phosphoethanolamine-N-(lissamine  
12 rhodamine B sulfonyl, ammonium salt) (DPPE-Rhod.) in powder form was obtained from the same company.  
13 The salts and buffering agents (all > 99.0% purity) were purchased from Sigma-Aldrich (Dorset, UK) and  
14 dissolved/diluted in ultrapure water (Merck-Millipore, Watford, UK). Solutions were created with fixed  
15 concentrations of ions as follow: KCl 150 mM, NaCl 150 mM, Tris 10 mM, CaCl<sub>2</sub> 2 mM, combining them in  
16 the eight different solutions listed in Table 1. Wherever possible, the pH was adjusted to 7.4 using HCl 5 M and  
17 KOH/NaOH 5 M (depending on whether NaCl or KCl was used in the solution).

18

Solution ref. number	Solution composition
1	KCl 150 mM
2	NaCl 150 mM
3	Tris 10 mM / NaCl 150 mM
4	Tris 10 mM / KCl 150 mM
5	NaCl 150 mM / CaCl <sub>2</sub> 2 mM
6	KCl 150 mM / CaCl <sub>2</sub> 2 mM
7	Tris 10 mM / NaCl 150 mM / CaCl <sub>2</sub> 2 mM
8	Tris 10mM / KCl 150mM / CaCl <sub>2</sub> 2mM

19

20 **TABLE 1** Detailed composition of the eight different deposition solutions used for the formation of SLBs. The measurement  
21 solutions were obtained in each case by diluting 15 times the preparation solutions with ultrapure water.

22

### 23 Supported lipid bilayer preparation

24 Supported lipid bilayers (SLBs) of DOPC, POPC and DOPS were formed via the vesicle fusion method (13,  
25 64). In short, 100  $\mu$ L of a chloroform solution containing the lipids (10 mg/mL for DOPC and POPC, and 1  
26 mg/mL for DOPS) was pipetted into a 3 mL glass vial and dried under a gentle nitrogen steam until no fluid  
27 remained. For FRAP experiments, 1.6  $\mu$ L of DPPE-Rhod 0.4 mM (0.05% final concentration) was added to the  
28 DOPC before drying. The vial was then placed under vacuum for > 12 hours to eliminate residual chloroform.  
29 The resulting lipid film was subsequently re-hydrated in 1 mL of the solution of interest so as to achieve a lipid  
30 concentration of 1 mg/mL. The vial was bath-sonicated for at least 30 minutes at > 40°C until the solution  
31 became uniformly milky and opaque due to the formation of multi-lamellar vesicles. The solution was then  
32 extruded 11 times using a Mini-Extruder kit (Avanti Polar Lipids Inc.) with a 100 nm filter (Whatman, Ge  
33 Healthcare Life Science, Amersham, UK) to form large unilamellar vesicles. The solution was further diluted 10  
34 times in the same solution (except DOPS), to reach a final concentration of 0.1 mg/mL. A drop (100  $\mu$ L) of this  
35 solution was deposited on a disc of Grade I freshly cleaved Muscovite mica (SPI supplies, West Chester, USA).  
36 The sample was incubated 30 minutes at 65°C in a sealed Petri dish and then progressively cooled down to 25°C  
37 over 1.5 hour to ensure full relaxation of the bilayer in its fluid state. The incubation was done in a water-  
38 saturated atmosphere to prevent any drying of the sample. The sample is then rinsed carefully with measurement  
39 solution (15 $\times$  diluted preparation solution) before AFM imaging. This last procedure serves two purposes: first  
40 since this study focuses on the influence of the substrate on the bilayer's behaviour, removal of some of the ions  
41 in solution emphasises the relative importance of the ions trapped between the bilayer and the substrate in

1 modulating SLB-substrate interactions. Second, the rinsing does not affect the already formed bilayer but it  
2 allows clearer images of the surface's changes and minimises tip-induced effects (65) (for details see Fig. S1).  
3 Since the DOPC bilayer is in fluid phase at the experimental temperature (25° C), any exposure of the sample to  
4 air (bubbles or drying) disrupts the bilayer assembly. It was therefore not possible to use a same bilayer for all  
5 the experiments (with solution exchange) and new samples were prepared for each experiment. All the  
6 glassware, and utensils used in the procedure were first thoroughly cleaned by sonication in, sequentially, an  
7 aqueous solution of Decon-90 detergent (Deacon Laboratories, Brighton, UK), ultrapure water, 20% isopropyl  
8 alcohol, and ultrapure water again, each time for ten minutes.

9 The antimicrobial peptide Temporin L (see below for details on the synthesis) was first equilibrated in Tris 10  
10 mM / NaCl 150 mM, pH 7.4 ± 0.2 stock solution at a concentration of 1.3 mM. Having the peptide solution  
11 already buffered at neutral pH avoids the pH-induced changes in the conformation of the peptide. In the  
12 comparative AFM analysis, 30 µL of the stock solution were added to the sample (100 µL), obtaining a final  
13 concentration of ~ 0.3 mM. When used in solution 6, the initial pH of the solution (6.0 ± 0.5) was brought near  
14 neutral value (pH 7.0 ± 0.2) by the adjunction of the peptide solution, allowing direct comparison between the  
15 different solutions without concerns for pH effects on the peptide structure. Solution 7 is already buffered and  
16 no measurable pH change was observed upon adjunction of Temporin (pH 7.4 ± 0.2).

### 18 Membrane penetrating peptide Temporin L synthesis

19 Peptide synthesis grade DMF was obtained from AGTC Bioproducts (Hessle, UK), PyBOP from Apollo  
20 Scientific (Stockport, UK) and all resins and amino acids were purchased from Novabiochem by Merck  
21 (Darmstadt, Germany). These chemicals were used without further purification and stored under appropriate  
22 conditions, as detailed in the manufacturer's instructions. Bond Elut solid phase extraction cartridges (20 mL,  
23 polypropylene with two polypropylene frits) were purchased from Crawford Scientific (Strathaven, UK) and  
24 used as reaction vessels for solid phase synthesis. Solvents were removed under reduced pressure using a Büchi  
25 Rotavapor R1 (Postfach, Switzerland), a shaker was used to mix solutions during solid phase synthesis and  
26 aqueous solutions were lyophilised using a Christ Alpha 1-2 LD Plus (Osterode am Harz, Germany) freeze-  
27 drier.

28 Temporin L (sequence FVQWFSKFLGRIL-NH<sub>2</sub>) was synthesised via manual solid phase peptide synthesis.  
29 Amino acid side chain functionality was protected as follows: FmocArg(Pbf)OH, FmocGln(Trt)OH,  
30 FmocLys(Boc)OH, FmocSer(tBu)OH and FmocTrp(Boc)OH. Fmoc-protected Rink Amide resin (0.1 mmol,  
31 128 mg, loading 0.78 mmol g<sup>-1</sup>) was swollen in DMF overnight at room temperature in a 20 mL polypropylene  
32 syringe fitted with two polyethylene frits. The resin was de-protected with piperidine (20 % in DMF v/v, 2 x 20  
33 min) and washed with DMF (3 x 2 mL). PyBOP (4 eq. with respect to the resin), the Fmoc-protected amino acid  
34 (4 eq.) and DIPEA (4 eq.) were dissolved in the minimum DMF and left to pre-activate for several minutes,  
35 before being added to the resin and placed on the shaker at 400 rpm at room temperature for 1 hour. The resin  
36 was then washed with DMF (3 x 2 mL) and de-protected using piperidine (20 % in DMF v/v, 2 x 20 min) and  
37 washed as before. Further amino acid couplings and Fmoc-deprotection steps were made as necessary to  
38 complete the full sequence. The resin was washed with DMF (3 x 2 mL) and then DCM (3 x 2 mL) to remove  
39 DMF prior to resin cleavage. Final cleavage from the resin was achieved using 95: 2.5: 2.5 TFA: H<sub>2</sub>O: TIPS (4  
40 mL). The resin was then placed on the shaker at 400 rpm for 4 hours and the resin removed by filtration. The  
41 cleavage cocktail was removed *in vacuo*, the crude product precipitated in diethyl ether (45 mL) and the  
42 precipitate retrieved by centrifuge for 15 min at 5000 rpm. The ether phase was decanted, the crude product  
43 dissolved in a mixture of acidified H<sub>2</sub>O and MeCN and lyophilised prior to RP-HPLC purification. The crude  
44 peptide was dissolved into ~1.5 mL (95 % H<sub>2</sub>O, 5 % MeCN, 0.1 % TFA) and purified by preparative RP-HPLC  
45 using a Perkin Elmer (Wokingham, UK) 200 Series LC pump with a Perkin-Elmer 785A UV-vis detector (λ =  
46 220 nm) on a SB Analytical column (ODS-H Optimal), 250 x 10 mm, 5 µm; flow rate = 2 mL min<sup>-1</sup>; typical  
47 linear gradient elution 0–100 % solvent B over 80 minutes, (solvent A = 0.1 % TFA in 95 % H<sub>2</sub>O, 5 % MeCN,  
48 solvent B = 0.1 % TFA in 5 % H<sub>2</sub>O, 95 % MeCN). Relevant fractions were collected, lyophilised and analysed  
49 by LC-MS and analytical RP-HPLC to yield Temporin L as a white powder (38 mg, 23 %); RP-analytical  
50 HPLC RT 17.8 min; approximate purity > 99 %; QToF MS mass calculated *m/z* [M+H]<sup>+</sup> 821.0, mass observed  
51 [M+2H]<sup>2+</sup> 820.7. The characterisation data described can be found in the Supporting Material (Fig. S2).

### 53 AFM measurements

1 A commercial AFM (Cypher ES, Asylum Research, Santa Barbara, CA) equipped with direct laser excitation  
2 (blueDrive) and temperature control was used for all the experiments. The blue drive and temperature control  
3 enable ultrastable operation and fully reproducible imaging parameters. This is important for allowing direct  
4 comparison between results acquired in the different imaging solutions. All measurements, except for the  
5 controls presented in Fig. S3, were conducted using cantilevers from a same wafer for better comparability  
6 (OMCL RC800-PSA, Olympus, Tokyo, Japan). The cantilevers have a nominal spring constant of 0.39 N/m and  
7 systematic thermal calibration (44, 66) showed variations of less than 10% between cantilevers. The tip is  
8 pyramidal shape with a curvature radius  $\leq 15$  nm at its apex. Imaging was carried out in amplitude modulation  
9 (AM) with the cantilever driven at its fundamental resonance frequency ( $\sim 25$  kHz in liquid) for all the  
10 experiments. In AM mode the cantilever is oscillated near resonance frequency and the amplitude is kept  
11 constant while scanning. The optical level sensitivity was calibrated before the experiments. The free amplitude  
12  $A_{free}$  away from the interface was set to  $A_{free} = 2.0$  nm. Images were acquired at setpoint amplitudes  $A_{set}$  of  
13 1.6, 1.2 and 0.6 nm for each sample, corresponding respectively to setpoint ratio  $A_{set}/A_{free}$  of 0.8 ('Soft'  
14 imaging conditions), 0.6 ('Medium' imaging conditions) and 0.3 ('Hard' imaging conditions). In all cases, it  
15 was ensure that the tip did not traverse the bilayer while oscillating. If such an event occurs, it can be  
16 immediately identified by dramatic changes in the resulting image due to the tip tapping the hard substrate  
17 underneath the SLB. For the control experiments shown in Fig. S3 a cantilever carrying a rounded tip (radius of  
18 curvature of  $\sim 30$  nm) made of the same material as the main tips was use (R30 FM, Nanosensors, Neuchatel,  
19 Switzerland).

20

## 21 Analysis of the AFM images

22

23 All the images were corrected for tilt (line or plane flattening) and lightly low-pass filtered to remove grainy  
24 noise using the WSxM software (Nanotec Electronica, Madrid, Spain) (67). Depending on the imaging solution,  
25 the membrane progressively became gel-like when decreasing the setpoint ratio (i.e. turning to 'Hard' imaging  
26 conditions). This transition induces the apparition of stable nano-features or nano-texturing of the membrane  
27 that remains in place throughout the imaging process. Quantification of the apparent surface structure was done  
28 with homemade routines programmed in Igor Pro (WaveMetrics, Lake Oswego, USA). Since objectively  
29 quantifying the degree of 'order' or the presence of 'stable' nanostructures is challenging, two different criteria  
30 were used to evaluate long-range and short-range lateral order respectively.

31 A first method, based on Fourier analysis was used to quantify the relative increase on long-range ( $> 150$  nm)  
32 order in the images, averaged over all directions. Long-range order is expected to increase significantly if the  
33 membrane undergoes a transition from fluid to gel-like. Here the analysis is done by examining the two-  
34 dimensional Fast Fourier Transforms (2D FFT) of height images. A profile is averaged over all directions and  
35 back-transformed into real space (see Fig. S4 A-C). The resulting curves (one per topographic image, Fig. S4 C)  
36 exhibit local maxima where features of a given size are more abundant in the original image. The change  $C_{FFT}$   
37 in long-range order is then calculated using:

$$C_{FFT} = \left| \int_{s1}^{s2} P_{FFT}^{Hard}(s) - P_{FFT}^{Soft}(s) ds \right| \quad (1)$$

38

39 where  $P_{FFT}^{Hard}$  and  $P_{FFT}^{Soft}$  are the averaged profiles for the images acquired in Hard and Soft conditions  
40 respectively, and  $s1, s2$  the interval in features sizes investigated. In  $P_{FFT}^{Hard}$ , local maxima are clearly visible for  
41 feature sizes that are multiples of  $\sim 20$  nm, the characteristic size of stress-induced gel-like protuberances.  
42 However, even when little stress is applied to the membrane (Soft and Medium conditions), some local maxima  
43 can be seen in the 10-50 nm size interval due to tip-induced fluctuations of the fluid membrane. The best  
44 indicator of membrane localised gelation is hence the existence of long-range order, obtained by taking [150  
45  $\mu\text{m}$ ; 300  $\mu\text{m}$ ] for the  $[s1; s2]$  interval.  $C_{FFT}$  is a quantitative indicator of the change in long-range order in a  
46 given sequence of images. However, its absolute value does not contain physically meaningful information and  
47  $C_{FFT}$  can hence be normalised to the largest value when comparing different sequences (as in Fig. 3).

48 The second method analyses the average correlation between adjacent linescans. It complements the Fourier  
49 analysis by quantifying the existence of short-range order, taking into account tip-induced fluctuations of a fluid  
50 membrane. If two adjacent profiles, as scanned by the tip, exhibit a high degree of similarity, then the resulting  
51 correlation will be close to unity (maximum value), regardless of the shape of the profile. Fluctuations over fluid  
52 membranes are hence likely to decrease the correlation (Fig. S4 D). Let's consider a height profile line

1  $P_{Corr}^{line\ n}(x)$  obtained from the raster scan line number  $n$  of the AFM tip over the image.  $x$  designates a point  
 2 along the profile. The image being 256 by 256 pixels, we have  $0 \leq n \leq 255$ . We define  $max_{line\ n}$ ,  $min_{line\ n}$   
 3 and  $avg_{line\ n}$  the numerical values of the maximum height, minimum height and average height of  $P_{Corr}^{line\ n}$ . We  
 4 can then define a normalised profile  $NP_{Corr}^{line\ n}$  as follow:  
 5

$$NP_{Corr}^{line\ n} = \frac{P_{Corr}^{line\ n} - avg_{line\ n}}{max_{line\ n} - min_{line\ n}} \quad (2)$$

6 This normalisation procedure ensures that each  $NP_{Corr}^{line\ n}$  is centred on zero (no vertical offset) and has a  
 7 maximum height variation of 1. We can then calculate the degree of correlation  $Corr_{n,n+1}$  between the two  
 8 adjacent lines  $n$  and  $n + 1$ :

$$Corr_{n,n+1} = 1 - \frac{\int_x |NP_{Corr}^{line\ n}(x) - NP_{Corr}^{line\ n+1}(x)| dx}{\int_x |NP_{Corr}^{line\ n}(x)| + |NP_{Corr}^{line\ n+1}(x)| dx} \quad (3)$$

9 where the integral is calculated over the whole length of the profile. Defined in this manner, we have  $0 \leq$   
 10  $Corr_{n,n+1} \leq 1$ , with  $Corr_{n,n+1} = 1$  corresponding to a situation where the two profiles are identical and the  
 11 values close to zero to a low degree of correlation. We note that other definitions of correlation are possible, but  
 12 the present definition has the advantage of being intrinsically normalised, with a simple interpretation of the  
 13 values obtained. We can then calculate a single correlation value  $Corr$  for any given image by averaging all the  
 14 correlation results  $Corr_{n,n+1}$  for  $0 \leq n < 255$ . The uncertainty is taken as the standard error.  
 15

16 Quantitative analysis of the image features was conducted on the raw data without any prior processing except  
 17 for tilt correction.  
 18

## 19 FRAP measurements

20 FRAP measurements were conducted on the DOPC SLBs in order to quantify lipid mobility in each solution. As  
 21 for AFM, the FRAP measurements were conducted after rinsing of the SLBs with a diluted solution. A  
 22 fluorescently labelled lipid (DPPE-Rhod, Avanti lipids) was added to the DOPC bilayer (0.05%). Its low  
 23 concentration does not affect the overall DOPC fluidity but the Rhodamine tag provides the fluorescence  
 24 needed. After the SLB formation, the sample was placed in an EZ-C1 Nikon Confocal Microscope (Nikon UK  
 25 Limited, Kingston, UK) and imaged in reflection mode. The fluorescence recovery was analysed over a  $10 \times 10$   
 26  $\mu m^2$  bleaching spot within a  $500 \times 500 \mu m^2$  image. We acquired 45 frames (1 second/frame, 2 seconds gap  
 27 between consecutive frames) over a total duration of 1 minute and 30 seconds. At least three frame sequences  
 28 were acquired for each sample so as to optimize the measurements parameters, ensure reliability of the result  
 29 and derive statistically meaningful results. The dark background was avoided to prevent modification of the  
 30 digital contrast. In cases where the bilayer did not cover the whole sample uniformly, we centred the bleaching-  
 31 spot at the centre of the largest as possible patches (see also Supporting Material, Fig. S5 for details).

32 The images sequences obtained from the FRAP measurements were processed with a user-defined macro  
 33 available in the software ImageJ (National Institutes of Health, USA). The resulting time-dependant  
 34 fluorescence intensity data were processed with in-built analysis tools in the software Igor Pro (WaveMetrics,  
 35 Lake Oswego, USA). The geometry of the bleaching spot being squared, the standard fitting equations (68)  
 36 normally used to derive the diffusion coefficient ( $D$ ) were adapted based on the derivation given in reference  
 37 (69) and used to fit time-dependent intensity data:

$$I(t) = a_0 + a_1 \left( 1 - \sqrt{\frac{w^2}{w^2 + 4\pi D(t - t_{bleach})}} \right) \quad (4)$$

38 where  $w$  (in  $\mu m$ ) is the width of the square spot area and  $D$  ( $\mu m^2/s$ ) is the diffusion coefficient of the lipid  
 39 molecules in the bilayer (see Fig. S5). The diffusion coefficients derived in each case were averaged over the  
 40 different sequences captured and the stated uncertainty is the standard error of the average. Higher uncertainties  
 41 values are found in presence of smaller SLB patches due to edge effects (see Supporting Material discussion  
 42 accompanying Fig. S5).  
 43  
 44

## 1 RESULTS AND DISCUSSION

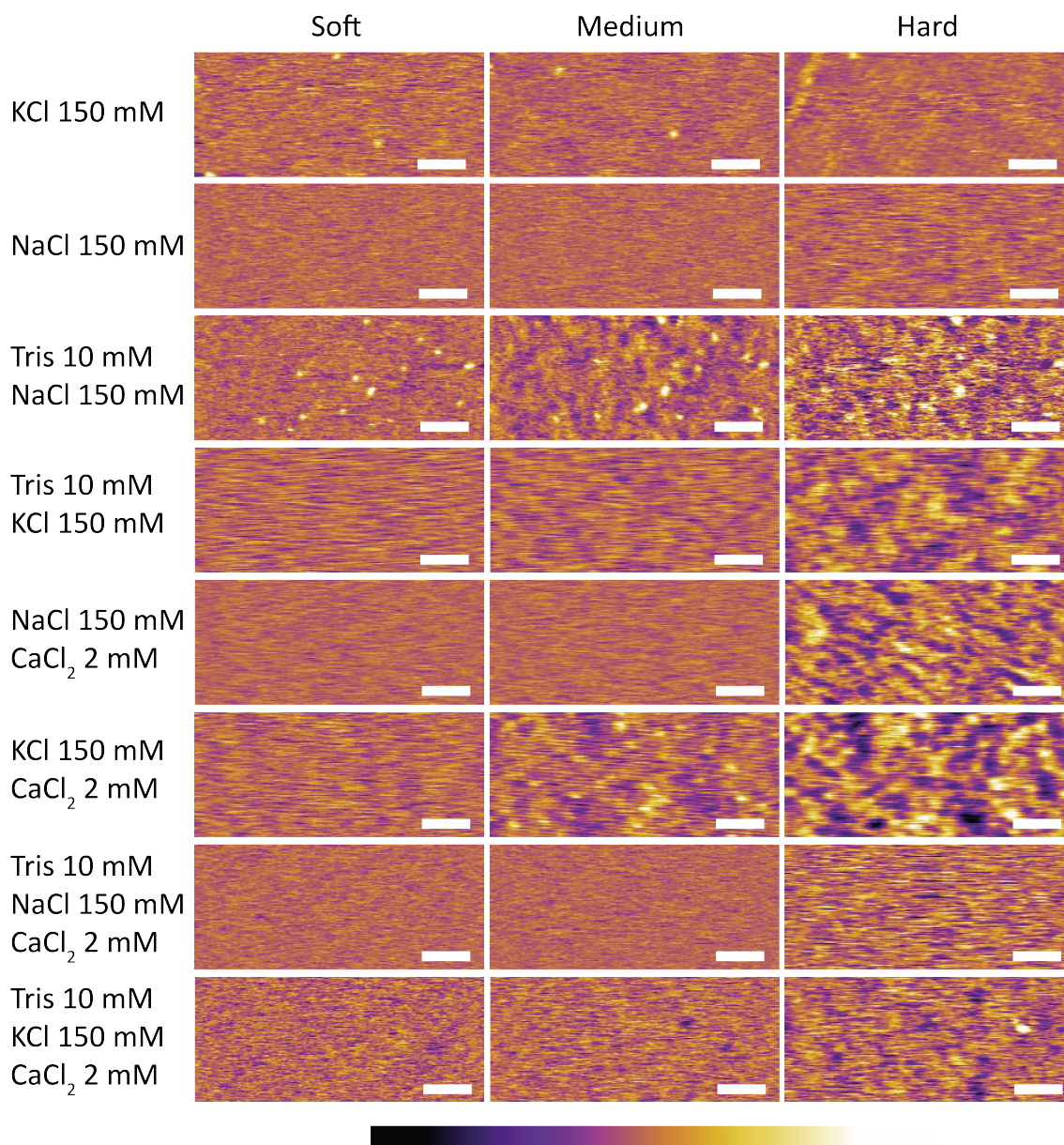
### 2 3 Mechanical stress induces ion-dependent nanoscale texturing of the bilayer

4  
5 Figure 1 shows representative AFM images of DOPC SLBs formed in the eight different saline solutions used.  
6 In each case, images acquired in scanning conditions described as ‘Soft’, ‘Medium’ and ‘Hard’ are given,  
7 corresponding to setpoint ratios of 0.8, 0.6, and 0.3 respectively (see Materials and Methods for details).

8 When imaged in Soft conditions, the average pressure exerted by the tip on the membrane is minimal and no  
9 particular features are visible, except for occasional protrusions due to un-fused vesicles. The membrane is fluid  
10 and the tip tends to sweep molecules as it scans across the surface, leading to relatively noisy images  
11 characteristic of AFM operation over fluid bilayers. As the imaging conditions progressively change from ‘Soft’  
12 to ‘Hard’, the average pressure exerted by the tip on the membrane increases and the appearance of the  
13 membrane can change dramatically, depending on the ionic content of the solution used for the bilayer  
14 formation. In order to emphasise the impact of ions in contact with the proximal leaflet (where the bilayer is  
15 supported), the SLB was rinsed with a diluted ionic solution (measurement solution) immediately before  
16 imaging (see Fig. S1). Using solutions containing only monovalent ions or divalent ions with Tris buffer little  
17 change is visible, as exemplified by solution 7 (Tris 10 mM / NaCl 150 mM / CaCl<sub>2</sub> 2 mM). In contrast, in  
18 solutions containing no Tris and divalent ions clear nanoscale structures start to emerge. This is particularly  
19 visible in solution 6 (KCl 150 mM / CaCl<sub>2</sub> 2 mM) where the bilayer surface orders itself in a corrugated profile  
20 composed of an extended network of 10-20 nm wide and ~0.8 nm deep valleys and ridges spanning the imaged  
21 area. These stable peaks and valleys create a nanoscale pattern hereafter referred as a ‘nano-texture’ for  
22 simplicity. These structures appear stable while the tip pressure is maintained and consecutive images acquired  
23 in Hard conditions show reproducible nanoscale features, despite DOPC being normally fluid at the  
24 experimental temperature of 25°C (transition temperature  $T_m = -17^\circ \text{C}$  in solution). This gel-like nano-texture  
25 appears almost instantaneously when pressure is applied by the scanning tip, pointing to a tip-induced effect.  
26 The stability of this nano-texture is reminiscent of a fluid to gel phase transition, hence our use of ‘gel-like’, but  
27 the present results do not characterise the nature of this transition. The texture eventually disappears if the tip is  
28 moved away from the surface of the membrane. This can be seen when changing scan conditions between  
29 consecutive images, suggesting a stress relaxation occurring over minutes (see Fig. S6). There is an apparent  
30 opposing action of Tris and CaCl<sub>2</sub>, both working in conjunction with the monovalent salts. When both species  
31 are present in the solution the fate of the membrane under stress becomes difficult to predict. Some subtle  
32 differences can be seen between the monovalent ions. There is, for example, a clearer texture definition in  
33 solution 3 than in solution 4, but between solution 5 and 6 the situation is reversed. Adjunction of cholesterol in  
34 the membrane only reinforces this effect (Fig. S7). This is hardly surprising given the different physico-  
35 chemical properties of cholesterol, but the result suggest that stress-induced nano-texturing may be a common  
36 feature of biological membranes.

37 Determining the origin of these nanostructures is not straightforward because the measurement process plays a  
38 role in their formation. Firstly, interactions between the imaging tip and the lipid bilayer can influence both the  
39 membrane and the observations. Here, to limit tip-induced disruption of the membrane, the AFM is operated in  
40 amplitude modulation, with the tip intermittently pressing the surface of the lipids. In contact mode, a similar  
41 nano-texture of the DOPC SLBs could be observed (Fig. S8 for an example in solution 6). However, the  
42 shearing motion of the tip in contact with the membrane renders this mode of imaging unstable and the tip tends  
43 to traverse the membrane even when using ultra-soft imaging conditions. In amplitude modulation, the imaging  
44 is fully stable. Depending on the imaging conditions (Soft, Medium or Hard) the tip probes the hydration  
45 landscape at the surface of the membrane or the nano-mechanical properties of the membrane itself (70, 71). In  
46 practice, this is quantitatively controlled by the imaging setpoint (see Material and Methods) that can be almost  
47 instantaneously re-adjusted at any time. In Hard imaging conditions, the setpoint is relatively low (about 30% of  
48 the free amplitude) and the tip transiently presses on the lipid surface during every oscillation cycle. Since the  
49 fast tip motion is vertical with respect to the lipid surface no significant shear is imposed. The nanoscale  
50 structures therefore appear to be induced by normal compression of the membrane, but the tip only dwells a few  
51 microseconds in a same location before moving on.

52



1  
2

3 FIGURE 1: Comparative analysis of representative AFM micrographs obtained on DOPC SLBs in each solution. The  
 4 average force exerted by the imaging tip on the SLB gradually increases as the scanning conditions change from ‘Soft’ to  
 5 ‘Medium’ to ‘Hard’ (corresponding respectively to setpoint values of 0.8, 0.6 and 0.3). The images acquired in solution 7  
 6 (Tris 10 mM / NaCl 150 mM / CaCl<sub>2</sub> 2 mM) exhibit little influence of the scanning conditions on the appearance of the  
 7 SLB’s surface. In contrast, images acquired in solution 6 (KCl 150 mM / CaCl<sub>2</sub> 2 mM), show an obvious increase in  
 8 surface roughness and the apparition of clear topographic ‘nano-texture’ as the setpoint decreases. All images scale bars are  
 9 50 nm and the colour scale bar represents a height variation of 0.8 nm.

10

11 Quantifying the maximum force  $F$  and the average pressure  $P$  locally applied by the tip to the SLB is  
 12 challenging. The tip oscillates at the resonance frequency of the cantilever, and its instantaneous deflection is  
 13 not directly related to the applied force (72, 73). Here, we are only interested in estimating the orders of  
 14 magnitude of  $F$  and  $P$  and therefore use the following approximation:  $F \sim kA_0(1 - S)$  where  $k$  is the spring  
 15 constant of the cantilever,  $A_0$  the free amplitude and  $S$  the setpoint ratio. This approximation yields  $F \sim 0.6$  nN in  
 16 Hard imaging conditions, so a force in the order of 0.1-1 nN, consistent with previous nano-mechanical studies

1 (73, 74). For the standard AFM tip, such a force induces a tip indentation depth of typically less than a  
2 nanometre in a biomembrane (74, 75). If we further assume that the contact area of the tip with the membrane is  
3 in the order of  $100 \text{ nm}^2$ , the local tip-induced pressure in the membrane is in the order of  $P \sim 1 - 10 \text{ MPa}$ . This  
4 pressure is comparable to the normal elasticity modulus (compressibility) of typical biomembranes (75, 76), and  
5 can be naturally induced by proteins able to locally alter the molecular arrangement of the lipids (77). Control  
6 experiments conducted with a tip presenting a radius of curvature twice as large revealed a similar nano-  
7 texturing of the membrane, although with smaller height variations due to the tip's size. Quantitative analysis of  
8 the features sizes indicated no significant difference between results obtained with the two different tips,  
9 suggesting that the features are intrinsic to the DOPC SLB and not due to tip convolution effects (Fig. S3).

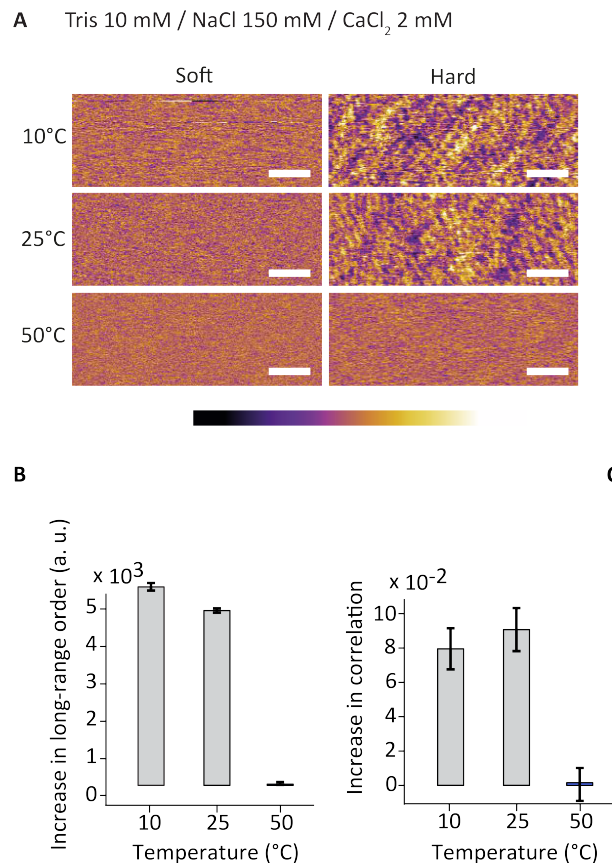
10  
11 Secondly, the strong influence of the solution in which the SLB is formed on the apparition of nano-texture  
12 points to ion-modulated substrate-lipid interactions. The local organization of the lipid molecules is dependent  
13 on the composition of the solution, provided the membrane is under a stress stimulus. This effect is also present  
14 if the experiment is carried out in the formation solution (Fig. S1) but it appears more clearly in the diluted  
15 solution (Fig. 1). Ionic species present in solution are known to influence specifically the mechanical and  
16 diffusion properties of the lipid bilayers (35), but to the best of our knowledge, no results available to date have  
17 examined the impact of the solution between the bilayer and its support, in particular mesoscale effects. Here,  
18 the particular stress-induced surface texture imaged by AFM suggest the lipids to behave similarly to “shear-  
19 thickening” liquids in rheology, with an effective viscosity determined by the ionic composition of the solution.  
20 The ions interact strongly enough with the lipids to trigger changes in their mobility within the membrane when  
21 under stress. Ion-mediated interactions between the lipids and the supporting substrate can in principle also  
22 stabilise the bilayer. It is known that several water layers are present between the lipids head-groups facing the  
23 mica (proximal leaflet) and the surface of the mica itself (32, 70). Ions must also be present in this region given  
24 their key role in modulating the bilayer deposition from vesicles in solution (78), and buffer ions can form  
25 nanoscale features on mica (79). However, these ionic features appear on a scale typically smaller than that  
26 observed here (79) and the membrane is generally fluid (15). The effect of the substrate can hence be seen as  
27 global and mostly homogenous with regard to the membrane properties, but local interactions could explain the  
28 spatial reproducibility of the textures observed over a same area. To distinguish the effect of the ions on the  
29 proximal and the distal (exposed) leaflet, we conducted some experiments where the SLB was formed in  
30 ultrapure water, and the liquid subsequently gently exchanged with a KCl and/or Tris solution known to induce  
31 considerable nano-texture under AFM imaging. Such texture appeared under tip pressure only when ions were  
32 in the solution, and disappeared completely after subsequent thorough rinsing with pure water. In contrast,  
33 bilayers prepared by directly re-hydrating the lipids in an ionic solution retained their ability to form textures  
34 even after several rinsing steps with water. This suggests a strong (almost irreversible) interaction between ions  
35 and the lipids, and confirms the limited influence of the substrate. In order to further support this finding, we  
36 have attempted to repeat our experiments on silicon oxide for its amorphous surface arrangement. The  
37 measurements were however inconclusive due to the intrinsic substrate's roughness which is comparable to that  
38 of the stress-induced texture on the bilayer (Fig. S9).

### 39 40 41 **Molecular origins of the stress-induced nano-texture**

42  
43 The results presented above demonstrate that the nano-texture induced by mechanical stress of the membrane is  
44 strongly dependent on the solution through ion-mediated substrate-lipid interactions. The results also show that  
45 the features composing this nano-texture are an intrinsic property of the DOPC SLB and do not significantly  
46 depend on the geometry of the AFM tip. Taken together, these findings hint at a local molecular rearrangement  
47 of the lipid when under stress so as to form solid-like nano ‘nodules’ that return to the initial fluid bilayer  
48 arrangement once the applied stress is removed. In other words, the bilayer could undergo a local fluid to gel-  
49 like transition when under stress, a process influenced by the ions' ability to modulate substrate-lipid and lipid-  
50 lipid interactions. It is well known that bilayers can exhibit ripples or corrugations induced mechanically (80),  
51 electrically (81) or by temperature when in pre-transition state (63, 82-84). These effects depend on various  
52 parameters such as head-group hydration, carbon chain length and ion species present in solution (85-87). Here  
53 similar effects seem at play but locally, on the nanometre scale. Stable surface texture indicates a high degree of  
54 molecular ordering within the bilayer, comparable to a highly localised pre-transition state. To verify this  
55 hypothesis, we conducted experiments similar to that presented in Fig. 1, but at different temperatures. The fluid  
56 to gel phase transition temperature of SLBs has been shown to increase by up to  $10 \text{ }^\circ\text{C}$  compared to the same

1 lipids in solution. The DOPC SLB remains fluid when imaged in Soft conditions, but if the AFM tip is able to  
 2 induce local gelation-like molecular ordering, a shift of 15 °C in the system temperature can be expected to have  
 3 a significant effect. We have therefore explored the behaviour of the SLB also at 10 °C and 50 °C for a solution  
 4 exhibiting limited stress-induced nano-texturing of the membrane (solution 7). The results, presented in Fig. 2  
 5 confirm that the tendency of the bilayer to form nano-texture increases at lower temperatures while the opposite  
 6 is true when the temperature is increased to 50 °C. This temperature dependence is consistent with the  
 7 hypothesis of stress-induced molecular ordering of the lipids, similar to a phase transition; the cooling limits  
 8 thermal excitation of the lipid molecules and favour gel-like molecular order in the membrane. The tip locally  
 9 increases the lipid-lipid proximity by momentarily confining the membrane and hence inducing local the  
 10 ordering (similar to gelation) more efficiently. The thermal vibrations of the lipid molecules increase with the  
 11 temperature, making it more difficult for the confining tip to induce the transition at 50 °C.

12



13  
14

15 FIGURE 2: AFM images of the evolution of DOPC SLBs on mica as a function of temperature (A). The SLB is formed in  
 16 solution 7 (Tris 10 mM / NaCl 150 mM / CaCl<sub>2</sub> 2 mM). The graphs (B) and (C) quantify the relative evolution of the stress-  
 17 induced nano-texture as a function of temperature. The existence of long-range order is given by FFT analysis (B) while  
 18 line-by-line correlation (C) quantifies short-range order on the membrane (see Materials and Methods and Fig. S4 for  
 19 details). In all cases, a significant decrease of order is visible at 50 °C. The images scale bar is 50 nm and the colour  
 20 scale bar represents a height variation of 0.8 nm.

21  
22

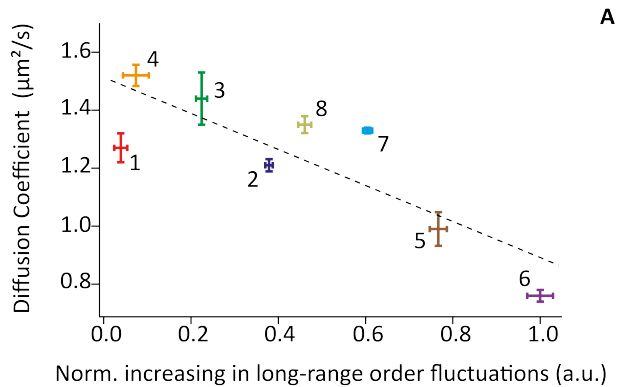
23 In order to analyse more quantitatively the tendency of a given system to undergo local gelation-like effects  
 24 under stress we used two different and complementary approaches (see Materials and Methods and Fig. S4 for  
 25 details). The first approach (Fig. 3 A) quantifies that relative increase in long-range order as the imaging  
 26 conditions change from Soft to Hard. Stable features should allow for improved longer-range order compared to  
 27 a fluctuating membrane. The quantification is done by integrating the long-range (> 150 nm) Fourier intensities  
 28 in all the directions of the reciprocal space (Fig. S4). The second approach quantifies short-range order by  
 29 examining the relative average increase in spatial correlation between two consecutive scan profiles upon a  
 30 change in scanning conditions. If the bilayer is in fluid state, two consecutive lines scan profiles will show little  
 31 correlation since surface features are mostly random. However, when gel-like texture appears, the degree of

1 correlation between adjacent profiles significantly increases. Both quantification approaches clearly support the  
2 qualitative observations derived from the AFM images.

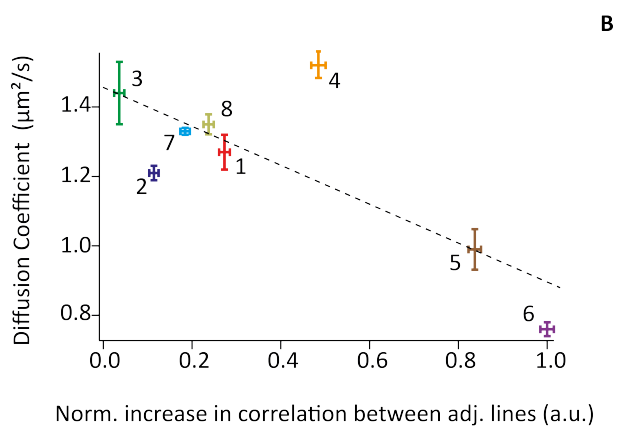
### 5 **Nano-texturing vs lipids mobility**

7 Stress and temperature both influence the phase transition in the SLB. The impact of the third parameter central  
8 to this study –the ionic content of the solution– is however less clear, beyond qualitative observations. It is  
9 obvious that ions can enhance or limit nano-texturing, but results can be confusing. For example, temperature  
10 studies such as that presented in Fig. 2 did not show conclusive results in certain solutions (Fig. S10). Similar  
11 inconclusive observations were made when replacing the phosphocholine zwitterionic lipid headgroup with a  
12 negatively charged phosphoserine that strongly binds cations (88, 89) (Fig. S11). This apparent complexity  
13 suggests that the ions cannot be considered in isolation, but their hydration properties as well as those of the  
14 lipids needs taking into consideration. In any case, it is clear that the mechanisms allowing specific ions or  
15 combination of ions to modulate substrate-lipid and lipid-lipid interactions is likely to take place at all time in  
16 solution, and not only when stress is applied with the AFM tip. If a given solution tends to enhance the  
17 formation of stress-induced nano-texture, its ions can be expected to stabilise lipid-lipid interactions within the  
18 SLB, effectively reducing the mobility of individual lipids molecules and bringing the bilayer closer to a gel  
19 transition. As for measurements at different temperatures, the action of the tip only provides a further reduction  
20 of mobility that would allow for a local transition similar to gelation to take place. To verify this hypothesis we  
21 conducted FRAP measurements over DOPC SLBs in each of the eight solutions (see Supporting Material, Fig.  
22 S5 for measurement details). The resulting diffusion coefficients in solution can then be examined against the  
23 tendency for stress-induced nano-texture over the same system, quantified using the two approaches described  
24 in the previous section (see Materials and Methods and Fig. S4 for details). The result is shown in Fig. 3 where  
25 the diffusion coefficient is plotted against the SLB's tendency to form stress-induced nano-texture, quantified  
26 with both analysis methods and in each solution.

27 Overall, the results shown in Fig. 3 support the hypothesis, namely the existence of an anti-correlation between  
28 lipid mobility and the formation of stress-induced nano-texture in the membrane. The low diffusion coefficients  
29 obtained in solutions 5 and 6 correlate with the significant texture intensity observed in AFM images under Hard  
30 conditions. In contrast, the ternary mixtures that induce the weakest AFM contrast exhibit relative high diffusion  
31 coefficients. Monovalent salts such as NaCl and KCl present significant differences in their diffusion  
32 coefficients when in association with CaCl<sub>2</sub> or with Tris. In any case, these results show that ions are able to  
33 locally control the mobility of lipids in a supported membrane also in the absence of mechanical stress or  
34 confinement. These observations are not limited to DOPC, and experiments conducted on biologically more  
35 relevant POPC (1-palmitoyl-2-oleoyl-sn-glycero-3-phosphocholine) bilayers revealed a very similar behaviour  
36 (see Fig. S12). This confirms the generality of our findings, at least for phosphocholine-based SLBs. The  
37 combination of these findings with, previously described, stress-induced nano texturing effect unveils the  
38 possibility of for ion-induced clusters of lipids molecules to exist naturally in the membrane, and act as diffusion  
39 units at the mesoscale. In this picture, the AFM only enhances the already existing nanostructure by applying  
40 mechanical stress. It is, however, not possible to distinguish whether the AFM tip induces or simply reveals the  
41 nano-texture solely based on the present data. AFM measurements are fundamentally perturbative in nature, and  
42 we cannot exclude possible unexpected effects of the AFM tip on the system, especially in the absence of  
43 independent experimental confirmation.



1. KCl 150 mM
2. NaCl 150 mM
3. Tris 10 mM / NaCl 150 mM
4. Tris 10 mM / KCl 150 mM
5. NaCl 150 mM /  $\text{CaCl}_2$  2 mM
6. KCl 150 mM /  $\text{CaCl}_2$  2 mM
7. Tris 10 mM / NaCl 150 mM /  $\text{CaCl}_2$  2 mM
8. Tris 10 mM / KCl 150 mM /  $\text{CaCl}_2$  2 mM



1  
2  
3  
4  
5  
6  
7  
8  
9  
10

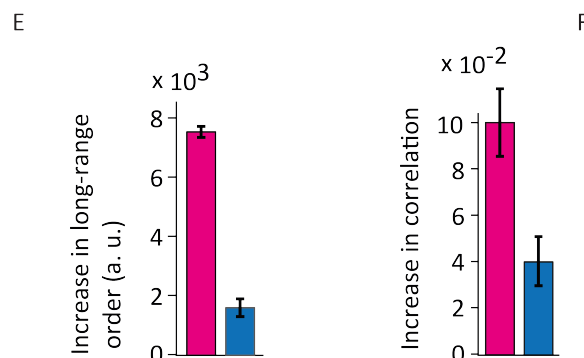
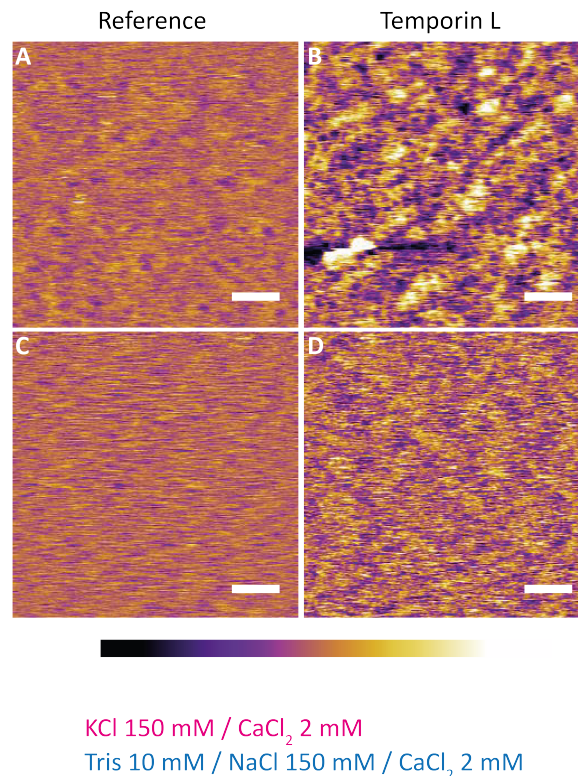
FIGURE 3 Graphs of the lipid diffusion coefficient values in all the eight different solutions plotted against the tendency of the membrane to form nano-texture when under mechanical stress. The two graphs are for the two quantification methods of the stress-induced nano-texturing tendency. The first graph (A) gives the diffusion coefficient against the relative increase in long-range ( $> 150$  nm) order as the imaging conditions change from Soft to Hard, derived from Fourier analysis. The second graph (B) shows the diffusion coefficient against the relative change in spatial correlation between two consecutively acquired line scan profiles as the imaging conditions change from Soft to Hard. The error bars represent the standard error of each measurement. The dotted lines are linear fits of the data. Details of the analysis are given in Materials and Methods and in Figs. S4 and S5.

11  
12  
13  
14  
15  
16  
17  
18  
19  
20  
21  
22

### Impact of nano-texturing on interacting biomolecules

The results of the last section clearly show that, depending on the ionic composition of the solution between the membrane and its support, the local viscoelastic properties of the bilayer can change significantly. The AFM experiments suggest that this change is not uniform at the molecular level, but rather involves mesoscale lipid clusters on the 20-50 nm range. Practically, the existence of ion-modulated mesoscale variations in fluid bilayers' properties could play an important role in controlling molecular processes in the membrane, for example spatially guiding dissolved chemicals and biomolecules to certain locations of the membrane, or preventing/enhancing adsorption near supported location. This idea is difficult to verify for natural biomembranes given their complexity, but we tested the underlying principle by examining the spatial details of

1 how cell-penetrating peptides insert into DOPC SLBs exposed to solutions promoting or limiting nano-texturing  
 2 (solutions 6 and 7, respectively). We use a well-known antimicrobial peptide, Temporin L for this experiment.  
 3 Temporin L was first isolated from the skin secretion of the European red frog *Rana temporaria* (90, 91).  
 4 Temporin L disrupts plasma membranes inducing cell death in bacteria (92) and parasites (93, 94). The results,  
 5 shown in Fig. 4 confirm the idea: the adsorption of Temporin L significantly differs in solution 6 compared to  
 6 solution 7, even when imaged in Soft conditions. (Fig. 4 B and D, respectively). In solution 6, the high degree of  
 7 similarity between the stress-induced (Fig. 1) and Temporin L-induced (Fig. 4 B) nano-textures in the bilayer  
 8 strongly suggests a correlation: the ionic solution can locally modify the properties of the bilayer, which in turn  
 9 modulate localise adsorption of the peptide. In contrast, the bilayer structure induced by Temporin L adsorption  
 10 is less clear in solution 7, despite an increase in long-range order indicating that the membrane is more solid-like  
 11 (Fig. 4 D).  
 12



13  
 14  
 15 FIGURE 4: Impact of ions in solution on the adsorption of Temporin L into DOPC SLBs. Two solutions are compared:  
 16 solution 6 (KCl 150 mM / CaCl<sub>2</sub> 2 mM) (A-B) and solution 7 (Tris 10 mM / NaCl 150 mM / CaCl<sub>2</sub> 2 mM) (C-D). All the  
 17 AFM images are taken in Soft imaging condition. The apparition of stable textures in topography is caused by the insertion  
 18 of Temporin L into the SLB. The process appears dependent on the type of solution in which the experiment takes place. The  
 19 more pronounced surface texturing is obtained in the solution inducing the largest stress-induced texturing of the pure SLB.  
 20 In both cases, pH effects can be ruled out (see Materials and Methods). The images scale bar is 50 nm and the colour scale  
 21 bar represents a height variation of 0.8 nm.

## 1 **General discussion**

2  
3 Taken together, the results presented in this paper suggest that ions can locally order fluid membranes on the  
4 mesoscale through interactions involving primarily the lipid headgroups. The effect is particularly strong for  
5 SLBs, where ions and water molecules located between the membrane and the support can form a more ordered  
6 hydrogen bond network due to spatial confinement (33). The fact that these lipid-ion interactions involve  
7 specific ions and are not enhanced with charged phosphoserine headgroups suggest that electrostatics alone is  
8 not sufficient to explain the observations, but rather the interacting hydration shells of both the dissolved ions  
9 and the headgroups (95). This is further supported by the fact that similar results were obtained with DOPC and  
10 POPC SLBs, confirming that interactions between the lipid tails do not dominate the local molecular ordering in  
11 the bilayer investigated here. These findings are compatible with previous studies over similar systems where  
12 ion-modulated membrane cohesion was found for symmetrically exposed bilayers (85-87, 95). Here the results  
13 are dominated by the effect of ions on the proximal leaflet, but the tendency nonetheless stands (96, 97). The  
14 asymmetry induced by substrate interactions can influence the phase-transition temperature of membranes (97),  
15 as well as natural membrane fluctuations (96), and lipids microdomain diffusion (98). Our investigations  
16 integrate these studies and highlight the specific effect of ion-mediated substrate interactions on the lipids'  
17 diffusion and stress-induced nano-texturing. In the absence of mechanical stress, the membrane remains fluid,  
18 but with a diffusion coefficient that depends on the ions in solution. We propose that this can be understood as  
19 due to the existence of transient lipid clusters, effectively acting as the membrane diffusion units. In this picture,  
20 the clusters are held together by the ion-mediated hydration interactions between lipid headgroups with other  
21 lipids and the substrate, and their size is on the same order as the spatial texture seen by AFM. Imposing a local  
22 stress with the AFM tip does not induce mesoscale molecular ordering, but only reinforces it to the point where  
23 local transition similar to gelation can occur over the area scanned by the tip. Practically, this gives rise to the  
24 characteristic solid-like nano-texture reported in this paper.

25 Although more work is needed to fully confirm the proposed picture, our results already suggest intriguing  
26 possibilities for the function of natural biological membranes. First, the existence of mesoscale order has  
27 consequences for the local dynamics induced by the support of fluid membranes; local lipid clusters naturally  
28 alter both the mechanical properties of the membrane and its ability to respond to external constraints such as  
29 changes in shape. The same mechanisms could also play a role for the formation of transient proteins and lipid  
30 clusters in the membrane, in particular when considering the debated topic of rafts (63, 84, 99). An important  
31 aspect of this picture is its independence on energy which would make it an efficient amplification mechanism  
32 for membrane proteins able to locally induce mechanical stress in the membrane. Second, depending on the ions  
33 in contact with the membrane and the supporting structure, chemicals and biomolecules in solution will not  
34 interact with each location of the membrane equally, but some spatial modulation will take place. This is  
35 exemplified here by the spatially modulated adsorption of a peptide into the DOPC SLB (Fig. 4). Further work  
36 will establish the extent to which these effects impact complex natural membranes.

## 37 38 39 40 **CONCLUSION**

41 In this paper, we report how different ionic solutions can modulate the nanoscale properties of supported fluid  
42 lipid bilayers, allowing local ordering and clustering of the lipid molecules, and promoting stress-induced local  
43 gel-like molecular ordering. When observed at the nanoscale, the stress-induced local transitions appear as a  
44 nano-texture induced by nodules with a characteristic length-scale of 20-30 nm. Combining atomic force  
45 microscopy in liquid and fluorescence recovery after photobleaching measurements, we correlate the well-  
46 known macroscopic effect of ions on lipid mobility in DOPC bilayers with the lipids tendency to form nano-  
47 texture that we attribute to local ordering in the membrane mediated by the water and ions trapped between the  
48 bilayer and its support. Our results highlight a clear but complex interplay between ions, hydration water,  
49 substrate, and lipid dynamics at the nanoscale with potentially important consequences for biological  
50 membranes. We illustrate this last point by showing that the interaction of peptides with DOPC bilayers is  
51 spatially modulated following a similar pattern to the stress-induced nano-texture of the membrane in the same  
52 solution in the absence of the peptide. Significantly, we show that ions alone are able to modulate the properties  
53 of bilayers over characteristic mesoscopic length-scales, resulting in complex membrane behaviour without any  
54 need for additional energy-dependant processes such as shepherding proteins. We believe our findings could

1 have significant implications for understanding the behaviour of biological membranes, in particular the active  
2 role played by lipids in supporting biological function.

### 5 SUPPORTING MATERIAL

6 Additional figures and discussion describing complementary measurements and control experiments are  
7 available at [www.cell.com](http://www.cell.com).

### 9 AUTHOR CONTRIBUTIONS

10 L.P. and K.V. conceived the study and designed the experiments. The measurements were conducted by L.P.,  
11 K.V. analysed the data and H.L.B.-N.R. synthesized the peptide. L.P. and K.V. wrote the manuscript with  
12 contributions from S.C. and H.L.B.

### 14 ACKNOWLEDGEMENTS

15 We thank Dr. Amir Farokh Payam and William Trewby (University of Durham, Physics Department) for help  
16 with mathematical analysis and Ethan J. Miller (University of Durham, Physics Department) for his assistance  
17 in the FRAP experiments. This research was supported by the Engineering and Physical Sciences Research  
18 Council (grant EP/M023915/1), the Biotechnology and Biological Sciences Research Council (grant  
19 BB/M024830/1) and Durham University (DTG, HLB).

### 21 SUPPORTING CITATIONS

22 References (100-105) appear in the Supporting Material.

### 23 REFERENCES

- 24 1. Cooper, G. M., and R. E. Hausman. 2016. The Cell: A Molecular Approach. In *The Cell: A Molecular*  
25 *Approach*. Sinauer Associates.
- 26 2. Singer, S. J., and G. L. Nicolson. 1972. Fluid Mosaic Model of Structure of Cell-Membranes. *Science*.  
27 175:720-&.
- 28 3. Bagatolli, L. A., J. H. Ipsen, A. C. Simonsen, and O. G. Mouritsen. 2010. An outlook on organization  
29 of lipids in membranes: Searching for a realistic connection with the organization of biological  
30 membranes. *Progress in Lipid Research*. 49:378-389.
- 31 4. Carquin, M., L. D'Auria, H. Pollet, E. R. Bongarzone, and D. Tyteca. 2016. Recent progress on lipid  
32 lateral heterogeneity in plasma membranes: From rafts to submicrometric domains. *Progress in Lipid*  
33 *Research*. 62:1-24.
- 34 5. Chiantia, S., and E. London. 2012. Acyl Chain Length and Saturation Modulate Interleaflet Coupling  
35 in Asymmetric Bilayers: Effects on Dynamics and Structural Order. *Biophys. J.* 103:2311-2319.
- 36 6. Nickels, J. D., J. C. Smith, and X. L. Cheng. 2015. Lateral organization, bilayer asymmetry, and inter-  
37 leaflet coupling of biological membranes. *Chem. Phys. Lipids*. 192:87-99.
- 38 7. Zimmerberg, J., and M. M. Kozlov. 2006. How proteins produce cellular membrane curvature. *Nat.*  
39 *Rev. Mol. Cell Biol.* 7:9-19.
- 40 8. van Meer, G., D. R. Voelker, and G. W. Feigenson. 2008. Membrane lipids: where they are and how  
41 they behave. *Nat. Rev. Mol. Cell Biol.* 9:112-124.
- 42 9. Gambin, Y., M. Reffay, E. Sierrecki, F. Homble, R. S. Hodges, N. S. Gov, N. Taulier, W. Urbach. 2010.  
43 Variation of the lateral mobility of transmembrane peptides with hydrophobic mismatch. *J. Phys.*  
44 *Chem. B.* 114:3559-3566.
- 45 10. Pincet, F., V. Adrien, R. Yang, J. Delacotte, J. E. Rothman, W. Urbach, and D. Tareste. 2016. FRAP to  
46 Characterize Molecular Diffusion and Interaction in Various Membrane Environments. *PloS One*.  
47 11:e0158457.
- 48 11. Jacobson, K., O. G. Mouritsen, and R. G. W. Anderson. 2007. Lipid rafts: at a crossroad between cell  
49 biology and physics. *Nat. Cell Biol.* 9:7-14.
- 50 12. Cremer, P. S., and S. G. Boxer. 1999. Formation and spreading of lipid bilayers on planar glass  
51 supports. *J. Phys. Chem. B.* 103:2554-2559.
- 52 13. Richter, R., A. Mukhopadhyay, and A. Brisson. 2003. Pathways of lipid vesicle deposition on solid  
53 surfaces: A combined QCM-D and AFM study. *Biophys. J.* 85:3035-3047.
- 54 14. Akesson, A., T. Lind, N. Ehrlich, D. Stamou, H. Wacklin, and M. Cardenas. 2012. Composition and  
55 structure of mixed phospholipid supported bilayers formed by POPC and DPPC. *Soft Matter*. 8:5658-  
56 5665.

- 1 15. Veatch, S. L., and S. L. Keller. 2003. Separation of liquid phases in giant vesicles of ternary mixtures  
2 of phospholipids and cholesterol. *Biophys. J.* 85:3074-3083.
- 3 16. Ashkar, R., M. Nagao, P. D. Butler, A. C. Woodka, M. K. Sen, and T. Koga. 2015. Tuning membrane  
4 thickness fluctuations in model lipid bilayers. *Biophys. J.* 109:106-112.
- 5 17. Bradley, R. P., and R. Radhakrishnan. 2016. Curvature-undulation coupling as a basis for curvature  
6 sensing and generation in bilayer membranes. *Proc. Natl. Acad. Sci. U. S. A.* 113:E5117-5124.
- 7 18. Johnson, S. J., T. M. Bayerl, D. C. McDermott, G. W. Adam, A. R. Rennie, R. K. Thomas, and E.  
8 Sackmann. 1991. Structure of an adsorbed dimyristoylphosphatidylcholine bilayer measured with  
9 specular reflection of neutrons. *Biophys. J.* 59:289-294.
- 10 19. Picas, L., P. E. Milhiet, and J. Hernandez-Borrell. 2012. Atomic force microscopy: a versatile tool to  
11 probe the physical and chemical properties of supported membranes at the nanoscale. *Chem. Phys.*  
12 *Lipids.* 165:845-860.
- 13 20. Machan, R., and M. Hof. 2010. Lipid diffusion in planar membranes investigated by fluorescence  
14 correlation spectroscopy. *Biochim. Biophys. Acta.* 1798:1377-1391.
- 15 21. Kam, L. C. 2009. Capturing the nanoscale complexity of cellular membranes in supported lipid  
16 bilayers. *J. Struct. Biol.* 168:3-10.
- 17 22. Melzak, K. A., S. Moreno-Flores, A. E. Lopez, and J. L. Toca-Herrera. 2011. Why size and speed  
18 matter: frequency dependence and the mechanical properties of biomolecules. *Soft Matter.* 7:332-342.
- 19 23. Wu, H.-L., H.-K. Tsao, and Y.-J. Sheng. 2016. Dynamic and mechanical properties of supported lipid  
20 bilayers. *J. Chem. Phys.* 144:154904.
- 21 24. Giménez, D., O. L. Sánchez-Muñoz, and J. Salgado. 2015. Direct Observation of Nanometer-Scale  
22 Pores of Melittin in Supported Lipid Monolayers. *Langmuir.* 31:3146-3158.
- 23 25. Rapson, Andrew C., Mohammed A. Hossain, John D. Wade, Edouard C. Nice, Trevor A. Smith,  
24 Andrew H. A. Clayton, and Michelle L. Gee. 2011. Structural Dynamics of a Lytic Peptide Interacting  
25 with a Supported Lipid Bilayer. *Biophys. J.* 100:1353-1361.
- 26 26. Wu, J.-C., P.-Y. Tseng, W.-S. Tsai, M.-Y. Liao, S.-H. Lu, C. W. Frank, J.-S. Chen, H.-C. Wu, Y.-C.  
27 Chang. 2013. Antibody conjugated supported lipid bilayer for capturing and purification of viable  
28 tumor cells in blood for subsequent cell culture. *Biomaterials.* 34:5191-5199.
- 29 27. Lee, Y. K., S. Kim, and J.-M. Nam. 2015. Dark-Field-Based Observation of Single-Nanoparticle  
30 Dynamics on a Supported Lipid Bilayer for In Situ Analysis of Interacting Molecules and  
31 Nanoparticles. *ChemPhysChem.* 16:77-84.
- 32 28. Horvath, R., B. Kobzi, H. Keul, M. Moeller, and É. Kiss. 2013. Molecular Interaction of a New  
33 Antibacterial Polymer with a Supported Lipid Bilayer Measured by an in situ Label-Free Optical  
34 Technique. *Int. J. Mol. Sci.* 14:9722-9736.
- 35 29. Sarangi, N. K., and A. Patnaik. 2012. L-Tryptophan-Induced Electron Transport across Supported  
36 Lipid Bilayers: an Alkyl-Chain Tilt-Angle, and Bilayer-Symmetry Dependence. *ChemPhysChem.*  
37 13:4258-4270.
- 38 30. Becucci, L., D. Valensin, M. Innocenti, and R. Guidelli. 2014. Dermcidin, an anionic antimicrobial  
39 peptide: influence of lipid charge, pH and Zn<sup>2+</sup> on its interaction with a biomimetic membrane. *Soft*  
40 *Matter.* 10:616-626.
- 41 31. Jacobson, K., and D. Papahadjopoulos. 1975. Phase transitions and phase separations in phospholipid  
42 membranes induced by changes in temperature, pH, and concentration of bivalent cations.  
43 *Biochemistry.* 14:152-161.
- 44 32. Anderson, T. H., Y. J. Min, K. L. Weirich, H. B. Zeng, D. Fygenson, and J. N. Israelachvili. 2009.  
45 Formation of Supported Bilayers on Silica Substrates. *Langmuir.* 25:6997-7005.
- 46 33. Tero, R. 2012. Substrate Effects on the Formation Process, Structure and Physicochemical Properties  
47 of Supported Lipid Bilayers. *Materials.* 5:2658.
- 48 34. Dekkiche, F., M. C. Corneci, A. M. Trunfio-Sfarghiu, B. Munteanu, Y. Berthier, W. Kaabar, and J. P.  
49 Rieu. 2010. Stability and tribological performances of fluid phospholipid bilayers: Effect of buffer and  
50 ions. *Colloids Surf., B.* 80:232-239.
- 51 35. Garcia-Manyes, S., G. Oncins, and F. Sanz. 2006. Effect of pH and ionic strength on phospholipid  
52 nanomechanics and on deposition process onto hydrophilic surfaces measured by AFM. *Electrochimi.*  
53 *Acta.* 51:5029-5036.
- 54 36. Bockmann, R. A., A. Hac, T. Heimburg, and H. Grubmuller. 2003. Effect of sodium chloride on a lipid  
55 bilayer. *Biophys. J.* 85:1647-1655.
- 56 37. Mao, Y., Y. Du, X. Cang, J. Wang, Z. Chen, H. Yang, and H. Jiang. 2013. Binding Competition to the  
57 POPG Lipid Bilayer of Ca<sup>2+</sup>, Mg<sup>2+</sup>, Na<sup>+</sup>, and K<sup>+</sup> in Different Ion Mixtures and Biological  
58 Implication. *J. Phys. Chem. B.* 117:850-858.

- 1 38. Gurtovenko, A. A., and I. Vattulainen. 2008. Effect of NaCl and KCl on phosphatidylcholine and  
2 phosphatidylethanolamine lipid membranes: Insight from atomic-scale simulations for understanding  
3 salt-induced effects in the plasma membrane. *J. Phys. Chem. B.* 112:1953-1962.
- 4 39. Lind, T. K., M. Cárdenas, and H. P. Wacklin. 2014. Formation of Supported Lipid Bilayers by Vesicle  
5 Fusion: Effect of Deposition Temperature. *Langmuir.* 30:7259-7263.
- 6 40. Reimhult, E., F. Hook, and B. Kasemo. 2003. Intact vesicle adsorption and supported biomembrane  
7 formation from vesicles in solution: Influence of surface chemistry, vesicle size, temperature, and  
8 osmotic pressure. *Langmuir.* 19:1681-1691.
- 9 41. Head, B. P., H. H. Patel, and P. A. Insel. 2014. Interaction of membrane/lipid rafts with the  
10 cytoskeleton: impact on signaling and function: membrane/lipid rafts, mediators of cytoskeletal  
11 arrangement and cell signaling. *Biochim. Biophys. Acta.* 1838:532-545.
- 12 42. Zhong, J., and J. Yan. 2016. Seeing is believing: atomic force microscopy imaging for nanomaterial  
13 research. *RSC Adv.* 6:1103-1121.
- 14 43. Takeshi, F. 2009. Subnanometer-Resolution Frequency Modulation Atomic Force Microscopy in  
15 Liquid for Biological Applications. *Jpn. J. of Appl. Phys.* 48:08JA01.
- 16 44. Miller, E. J., W. Trewby, A. F. Payam, L. Piantanida, C. Cafolla, and K. Voitchovsky. 2016. Sub-  
17 nanometer Resolution Imaging with Amplitude-modulation Atomic Force Microscopy in Liquid. *J.*  
18 *Visualized Exp.* (118), e54924, DOI:10.3791/54924.
- 19 45. Giocondi, M. C., D. Yamamoto, E. Lesniewska, P. E. Milhiet, T. Ando, and C. Le Grimmellec. 2010.  
20 Surface topography of membrane domains. *Biochim. Biophys. Acta.* 1798:703-718.
- 21 46. Hohlbauch, S. 2016. Nanomechanical and Viscoelastic Measurements in Biological Atomic Force  
22 Microscopy (AFM). *Biophys. J.* 110:498a-499a.
- 23 47. Dufrene, Y. F., and G. U. Lee. 2000. Advances in the characterization of supported lipid films with the  
24 atomic force microscope. *Biochim. Biophys. Acta, Biomembr.* 1509:14-41.
- 25 48. Chiantia, S., N. Kahya, J. Ries, and P. Schwille. 2006. Effects of Ceramide on Liquid-Ordered  
26 Domains Investigated by Simultaneous AFM and FCS. *Biophys. J.* 90:4500-4508.
- 27 49. Chiang, Y.-L., Y.-C. Chang, I. C. Chiang, H.-M. Mak, I.-S. Hwang, and Y.-L. Shih. 2015. Atomic  
28 Force Microscopy Characterization of Protein Fibrils Formed by the Amyloidogenic Region of the  
29 Bacterial Protein MinE on Mica and a Supported Lipid Bilayer. *Plos One.* 10:e0142506.
- 30 50. Ricci, M., R. A. Quinlan, and K. Voitchovsky. 2016. Sub-nanometre mapping of the aquaporin-water  
31 interface using multifrequency atomic force microscopy. *Soft Matter.*
- 32 51. Fukuma, T., M. J. Higgins, and S. P. Jarvis. 2007. Direct imaging of individual intrinsic hydration  
33 layers on lipid bilayers at Angstrom resolution. *Biophys. J.* 92:3603-3609.
- 34 52. Contera, S. A., K. Voitchovsky, and J. F. Ryan. 2010. Controlled ionic condensation at the surface of a  
35 native extremophile membrane. *Nanoscale.* 2:222-229.
- 36 53. Fukuma, T., M. J. Higgins, and S. P. Jarvis. 2007. Direct imaging of lipid-ion network formation under  
37 physiological conditions by frequency modulation atomic force microscopy. *Phys. Rev. Lett.*  
38 98:106101.
- 39 54. Ricci, M., P. Spijker, F. Stellacci, J.-F. Molinari, and K. Voitchovsky. 2013. Direct Visualization of  
40 Single Ions in the Stern Layer of Calcite. *Langmuir.* 29:2207-2216.
- 41 55. Ricci, M., W. Trewby, C. Cafolla, and K. Voitchovsky. 2017. Direct observation of the dynamics of  
42 single metal ions at the interface with solids in aqueous solutions. *Sci. Rep.* 7:43234.
- 43 56. Voitchovsky, K., J. J. Kuna, S. A. Contera, E. Tosatti, and F. Stellacci. 2010. Direct mapping of the  
44 solid-liquid adhesion energy with subnanometre resolution. *Nat. Nanotechnol.* 5:401-405.
- 45 57. Evert, L. L., D. Leckband, and J. N. Israelachvili. 1994. Structure and Dynamics of Ion-Induced  
46 Domains in Free and Supported Monolayers and Bilayers. *Langmuir.* 10:303-315.
- 47 58. Garcia-Manyes, S., G. Oncins, and F. Sanz. 2005. Effect of Ion-Binding and Chemical Phospholipid  
48 Structure on the Nanomechanics of Lipid Bilayers Studied by Force Spectroscopy. *Biophys. J.*  
49 89:1812-1826.
- 50 59. Dickey, A., and R. Faller. 2008. Examining the contributions of lipid shape and headgroup charge on  
51 bilayer behavior. *Biophys. J.* 95:2636-2646.
- 52 60. Marra, J., and J. Israelachvili. 1985. Direct measurements of forces between phosphatidylcholine and  
53 phosphatidylethanolamine bilayers in aqueous electrolyte solutions. *Biochemistry.* 24:4608-4618.
- 54 61. Bouvrais, H., L. Duelund, and J. H. Ipsen. 2014. Buffers Affect the Bending Rigidity of Model Lipid  
55 Membranes. *Langmuir.* 30:13-16.
- 56 62. Cevc, G., A. Watts, and D. Marsh. 1981. Titration of the phase transition of phosphatidylserine bilayer  
57 membranes. Effects of pH, surface electrostatics, ion binding, and head-group hydration. *Biochemistry.*  
58 20:4955-4965.
- 59 63. Dietrich, C., L. A. Bagatolli, Z. N. Volovyk, N. L. Thompson, M. Levi, K. Jacobson, and E. Gratton.  
60 2001. Lipid rafts reconstituted in model membranes. *Biophys. J.* 80:1417-1428.

- 1 64. Mingeot-Leclercq, M.-P., M. Deleu, R. Brasseur, and Y. F. Dufrene. 2008. Atomic force microscopy of  
2 supported lipid bilayers. *Nat. Protoc.* 3:1654-1659.
- 3 65. Ricci, M., P. Spijker, and K. Voitchovsky. 2014. Water-induced correlation between single ions  
4 imaged at the solid-liquid interface. *Nat. Commun.* 5.
- 5 66. Butt, H. J., and M. Jaschke. 1995. Calculation of thermal noise in atomic force microscopy.  
6 *Nanotechnology.* 6:1.
- 7 67. Horcas, I., R. Fernandez, J. M. Gomez-Rodriguez, J. Colchero, J. Gomez-Herrero, and A. M. Baro.  
8 2007. WSXM: a software for scanning probe microscopy and a tool for nanotechnology. *Rev. Sci.*  
9 *Instrum.* 78:013705.
- 10 68. Kang, M., C. A. Day, A. K. Kenworthy, and E. Di Benedetto. 2012. Simplified equation to extract  
11 diffusion coefficients from confocal FRAP data. *Traffic.* 13:1589-1600.
- 12 69. Blumenthal, D., L. Goldstien, M. Edidin, and L. A. Gheber. 2015. Universal Approach to FRAP  
13 Analysis of Arbitrary Bleaching Patterns. *Sci. Rep.* 5:11655.
- 14 70. Kunze, A., F. Zhao, A.-K. Marel, S. Svedhem, and B. Kasemo. 2011. Ion-mediated changes of  
15 supported lipid bilayers and their coupling to the substrate. A case of bilayer slip? *Soft Matter.* 7:8582.
- 16 71. Voitchovsky, K. 2013. Anharmonicity, solvation forces, and resolution in atomic force microscopy at  
17 the solid-liquid interface. *Phys. Rev. E.* 88.
- 18 72. Anczykowski, B., D. Krüger, K. L. Babcock, and H. Fuchs. 1996. Basic properties of dynamic force  
19 spectroscopy with the scanning force microscope in experiment and simulation. *Ultramicroscopy.*  
20 66:251-259.
- 21 73. Adamcik, J., A. Berquand, and R. Mezzenga. 2011. Single-step direct measurement of amyloid fibrils  
22 stiffness by peak force quantitative nanomechanical atomic force microscopy. *Appl. Phys. Lett.*  
23 98:193701.
- 24 74. Rico, F., C. Su, and S. Scheuring. 2011. Mechanical Mapping of Single Membrane Proteins at  
25 Submolecular Resolution. *Nano Lett.* 11:3983-3986.
- 26 75. Voitchovsky, K., S. Antoranz Contera, M. Kamihira, A. Watts, and J. F. Ryan. 2006. Differential  
27 stiffness and lipid mobility in the leaflets of purple membranes. *Biophys. J.* 90:2075-2085.
- 28 76. Perkins, M., S. J. Ebbens, S. Hayes, C. J. Roberts, C. E. Madden, S. Y. Luk, and N. Patel. 2007. Elastic  
29 modulus measurements from individual lactose particles using atomic force microscopy. *Int. J. Pharm.*  
30 *(Amsterdam, Neth.)* 332:168-175.
- 31 77. Phillips, R., T. Ursell, P. Wiggins, and P. Sens. 2009. Emerging roles for lipids in shaping membrane-  
32 protein function. *Nature.* 459:379-385.
- 33 78. Seantier, B., and B. Kasemo. 2009. Influence of Mono- And Divalent Ions on the Formation of  
34 Supported Phospholipid Bilayers via Vesicle Adsorption. *Langmuir.* 25:5767-5772.
- 35 79. Trewby, W., D. Livesey, and K. Voitchovsky. 2016. Buffering agents modify the hydration landscape  
36 at charged interfaces. *Soft Matter.* 12:2642-2651.
- 37 80. Alessandrini, A., and P. Facci. 2014. Phase transitions in supported lipid bilayers studied by AFM. *Soft*  
38 *Matter.* 10:7145-7164.
- 39 81. Li, M., M. Chen, E. Sheepwash, C. L. Brosseau, H. Li, B. Pettinger, H. Gruler, J. Lipkowski. 2008.  
40 AFM Studies of Solid-Supported Lipid Bilayers Formed at a Au(111) Electrode Surface Using Vesicle  
41 Fusion and a Combination of Langmuir-Blodgett and Langmuir-Schaefer Techniques. *Langmuir.*  
42 24:10313-10323.
- 43 82. Janiak, M. J., D. M. Small, and G. G. Shipley. 1976. Nature of the Thermal pretransition of synthetic  
44 phospholipids: dimyristoyl- and dipalmitoyllecithin. *Biochemistry.* 15:4575-4580.
- 45 83. Cevc, G. 1991. Polymorphism of the bilayer membranes in the ordered phase and the molecular origin  
46 of the lipid pretransition and rippled lamellae. *Biochim. Biophys. Acta.* 1062:59-69.
- 47 84. Leonenko, Z. V., E. Finot, H. Ma, T. E. S. Dahms, and D. T. Cramb. 2004. Investigation of  
48 Temperature-Induced Phase Transitions in DOPC and DPPC Phospholipid Bilayers Using  
49 Temperature-Controlled Scanning Force Microscopy. *Biophys. J.* 86:3783-3793.
- 50 85. Redondo-Morata, L., M. I. Giannotti, and F. Sanz. 2014. Structural impact of cations on lipid bilayer  
51 models: nanomechanical properties by AFM-force spectroscopy. *Mol. Membr. Biol.* 31:17-28.
- 52 86. Redondo-Morata, L., G. Oncins, and F. Sanz. 2012. Force spectroscopy reveals the effect of different  
53 ions in the nanomechanical behavior of phospholipid model membranes: the case of potassium cation.  
54 *Biophys. J.* 102:66-74.
- 55 87. Garcia-Manyes, S., L. Redondo-Morata, G. Oncins, and F. Sanz. 2010. Nanomechanics of lipid  
56 bilayers: heads or tails? *J. Am. Chem. Soc.* 132:12874-12886.
- 57 88. Martin-Molina, A., C. Rodriguez-Beas, and J. Faraudo. 2012. Effect of calcium and magnesium on  
58 phosphatidylserine membranes: experiments and all-atomic simulations. *Biophys. J.* 102:2095-2103.

- 1 89. Rodriguez, Y., M. Mezei, and R. Osman. 2007. Association free energy of  
2 dipalmitoylphosphatidylserines in a mixed dipalmitoylphosphatidylcholine membrane. *Biophys. J.*  
3 92:3071-3080.
- 4 90. Rinaldi, A. C., M. L. Mangoni, A. Rufo, C. Luzi, D. Barra, H. Zhao, P. K. J. Kinnunen, A. Bozzi, A. Di  
5 Giulio, M. Simmaco. 2002. Temporin L: antimicrobial, haemolytic and cytotoxic activities, and effects  
6 on membrane permeabilization in lipid vesicles. *Biochem. J.* 368:91-100.
- 7 91. Simmaco, M., G. Mignogna, S. Canofeni, R. Miele, M. L. Mangoni, and D. Barra. 1996. Temporins,  
8 antimicrobial peptides from the European red frog *Rana temporaria*. *Eur. J. Biochem.* 242:788-792.
- 9 92. Mangoni, M. L., N. Papo, D. Barra, M. Simmaco, A. Bozzi, A. Di Giulio, and A. C. Rinaldi. 2004.  
10 Effects of the antimicrobial peptide temporin L on cell morphology, membrane permeability and  
11 viability of *Escherichia coli*. *Biochem. J.* 380:859-865.
- 12 93. Cobb, S. L., and P. W. Denny. 2010. Antimicrobial peptides for leishmaniasis. *Curr. Opin. Invest.*  
13 *Drugs (BioMed Cent.)*. 11:868-875.
- 14 94. Eggimann, G. A., K. Sweeney, H. L. Bolt, N. Rozatian, S. L. Cobb, and P. W. Denny. 2015. The role  
15 of phosphoglycans in the susceptibility of *Leishmania mexicana* to the temporin family of anti-  
16 microbial peptides. *Molecules*. 20:2775-2785.
- 17 95. Melcrova, A., S. Pokorna, S. Pullanchery, M. Kohagen, P. Jurkiewicz, M. Hof, P. Jungwirth, P. S.  
18 Cremer, L. Cwiklik. 2016. The complex nature of calcium cation interactions with phospholipid  
19 bilayers. *Sci. Rep.* 6:38035.
- 20 96. Duro, N., M. Gjika, A. Siddiqui, H. L. Scott, and S. Varma. 2016. POPC Bilayers Supported on  
21 Nanoporous Substrates: Specific Effects of Silica-Type Surface Hydroxylation and Charge Density.  
22 *Langmuir*. 32:6766-6774.
- 23 97. Seeger, H. M., G. Marino, A. Alessandrini, and P. Facci. 2009. Effect of physical parameters on the  
24 main phase transition of supported lipid bilayers. *Biophys. J.* 97:1067-1076.
- 25 98. Sterling, Sarah M., R. Dawes, Edward S. Allgeyer, Sharon L. Ashworth, and David J. Neivandt.  
26 Comparison of Actin- and Glass-Supported Phospholipid Bilayer Diffusion Coefficients. *Biophys. J.*  
27 108:1946-1953.
- 28 99. Jacobson, K., O. G. Mouritsen, and R. G. Anderson. 2007. Lipid rafts: at a crossroad between cell  
29 biology and physics. *Nat. Cell Biol.* 9:7-14.
- 30 100. Muller, D. J., M. Amrein, and A. Engel. 1997. Adsorption of biological molecules to a solid support for  
31 scanning probe microscopy. *J. Struct. Biol.* 119:172-188.
- 32 101. Veatch, S. L., and S. L. Keller. 2002. Organization in lipid membranes containing cholesterol. *Phys.*  
33 *Rev. Lett.* 89:268101.
- 34 102. Stevens, M. M., A. R. Honerkamp-Smith, and S. L. Keller. 2010. Solubility Limits of Cholesterol,  
35 Lanosterol, Ergosterol, Stigmasterol, and beta-Sitosterol in Electroformed Lipid Vesicles. *Soft Matter*.  
36 6:5882-5890.
- 37 103. Ma, Y., S. K. Ghosh, D. A. DiLena, S. Bera, L. B. Lurio, A. N. Parikh, and S. K. Sinha. 2016.  
38 Cholesterol Partition and Condensing Effect in Phase-Separated Ternary Mixture Lipid Multilayers.  
39 *Biophys. J.* 110:1355-1366.
- 40 104. Almeida, P. F. 2011. A simple thermodynamic model of the liquid-ordered state and the interactions  
41 between phospholipids and cholesterol. *Biophys. J.* 100:420-429.
- 42 105. Gumi-Audenis, B., L. Costa, F. Carla, F. Comin, F. Sanz, and M. I. Giannotti. 2016. Structure and  
43 Nanomechanics of Model Membranes by Atomic Force Microscopy and Spectroscopy: Insights into  
44 the Role of Cholesterol and Sphingolipids. *Membranes (Basel, Switz.)*. 6.
- 45
- 46
- 47
- 48